Proceedings of the 21st ICSMGE, Vienna, Austria, 14 – 19 June 2026. Pistrol, Adam & Schweiger (eds.)
Published by: ÖGG, Austrian Society for Geomechanics, Salzburg, Austria, ISBN 978-3-9503898-4-5
https://doi.org/10.53243/ICSMGE2026-1553

Microstructure of non-plastic silty soils compacted at various moisture contents

Katarzyna Zabielska-Adamska, Dorota Małaszkiewicz
Faculty of Civil Engineering and Environmental Sciences, Bialystok University of Technology, Poland;
k.adamska@pb.edu.pl

Justyna Markowska
Doctoral School of Bialystok University of Technology, Poland

ABSTRACT: The paper aims to present the microstructure of compacted "transitional" soils: natural silty sand and fly ash with similar grain size distributions. Compacted transitional soils, macroscopically recognized as non-cohesive, are characterized by properties strictly dependent on the moisture content at compaction. Therefore, it is important to examine their microstructure. Samples were analyzed after compaction at three different water contents: at the optimum water content and on the dry and wet sides of the compaction curve. Microstructural studies were conducted based on ESEM images, which are considered the best for assessing soil microstructure in wet samples. The microstructures of two different non-plastic soils compacted at both sides of the optimum water content were determined using ESEM image analysis. A multi-modal structure was identified for fly ash compacted at $w \leq w_{opt}$, and a unimodal structure for compaction at $w > w_{opt}$. In the case of natural silty sand, a "transitional" nature of the structure was not evident; however, gap grading was concluded based on ESEM images.

KEYWORDS: Compacted soil, transitional soil, microstructure, pore size distribution, gap grading.

1 INTRODUCTION

In English-language publications, the behavior of sands is characterized by the fine content (f_C), which the ASTM D653:2024 standard describes as soil particles passing through a 0.075 mm sieve. According to ASTM D2487:2025, soil is considered fine-grained if at least 50% of the particles have a diameter smaller than 0.075 mm. Clays and silts meet this criterion. A more detailed classification of fine-grained soils is obtained by considering the plasticity index. However, soil that appears non-cohesive and non-plastic on a macroscopic level may still show properties of cohesive soils, not only in terms of strength but also deformation and filtration (Zabielska-Adamska 2020). This phenomenon is called mixed or transitional soil, and its properties after compaction depend heavily on the water content during compaction. Cubrinovski & Ishihara (2002), after testing over 300 natural sandy soils, stated that the threshold for structural change in sandy soil is a fines content of 30%. Beyond this, soils transition from a sand-dominated particle structure to a more fine-controlled structure, resembling cohesive soil properties.

Many researchers have performed tests on sand and fine fractions mixed in a laboratory in various proportions, among others, (Lade et al. 1998; Polito & Martin 2001; Nocilla et al. 2006; Kwa & Airey 2016). It should be noted that prepared mixtures of double-fraction soils create discontinuities in soil grain size distribution, and the difference between bimodal distributions increases as the ratio of the average diameters of both fractions grows (Lade et al. 1998). The soil behavior may depend on the amount of fine particles and the discontinuity in grain size. Wide gaps in the grain size distribution can significantly affect soil structure, as shown by comparing gap-graded sand-fines mixtures with natural sandy soils (Cubrinovski & Ishihara 2002). Ponzoni et al. (2017) stated that the presence of transitional behavior may depend on the hardness of the matrix material.

The paper aims to demonstrate the microstructure of compacted "transitional" soils on both sides of the optimum water content for natural silty sand and fly ash with similar grain size distributions, as observed through ESEM images. The authors' previous research (Zabielska-Adamska et al. 2019) confirms that fly ash microstructure on the dry and wet sides of optimum water content is similar to cohesive soils (Delage et al. 1996; Tarantino & De Col 2008; Romero 2013).

2 MATERIALS AND METHODS

2.1 *Materials*

The tests were conducted on two types of soil. The first was fly ash from the combustion of hard coal at the Bialystok Thermal-Electric Power Plant, stored in a dry storage yard. The basic mineralogical composition of fly ash is quartz (SiO_2), mullite ($3Al_2O_3 \cdot 2SiO_2$) and calcite ($CaCO_3$). The specific density (ρ_s) is 2.16 g/cm^3. The fly ash is a non-plastic material corresponding in grain size to sandy silt (saSi) with a median particle diameter (D_{50}) of 0.06 mm. The grain size distribution curve obtained for an average sample is presented in Figure 1. The coefficient of curvature, C_C=0.8, and the uniformity coefficient, C_U=4.0, indicate that fly ash is poorly graded (EN ISO 14688-2:2018). The fine content (f_C) is equal to 60%.

Natural soil is silty sand of Pleistocene origin (glaciofluvial deposit). It mainly consists of angular quartz grains. The specific density (ρ_s) is 2.68 g/cm^3. Tested soil is assessed (Figure 1) as a coarse soil (EN ISO 14688-1:2018), where the primary fraction is fine sand, and the secondary one is silt. The soil is silty sand (siSa) with a median particle diameter (D_{50}) of 0.077 mm and the fine content (f_C) of 47%. The grading coefficients indicate that silty sand is medium graded (C_U=6.8) or well graded (C_C=2.1). Based on the shape of the grain size distribution curve, it can be concluded that silty sand has a discontinuous grain size distribution, but this has not been confirmed by the standard.

2.2 *Methods*

Microstructural studies were performed using a FEI Quanta 250 FEG Scanning Electron Microscope in ESEM mode. Since the drying process may change the microstructure of the tested material, the images were taken using a gaseous SED (GSED) detector in ESEM mode, which enables samples to be observed with particular water content. The samples were tested directly after compaction. Samples were compacted dynamically in the oedometer ring to the densities corresponding to the points on the compaction curves $w_{opt} \pm 5\%$ obtained using the standard Proctor method.

Compaction curves for both tested soils are given in Figure 2. The physical parameters, such as water content (w), dry density (ρ_d), porosity (n), void ratio (e) and saturation degree (S_r) of the tested samples are shown in Table 1.

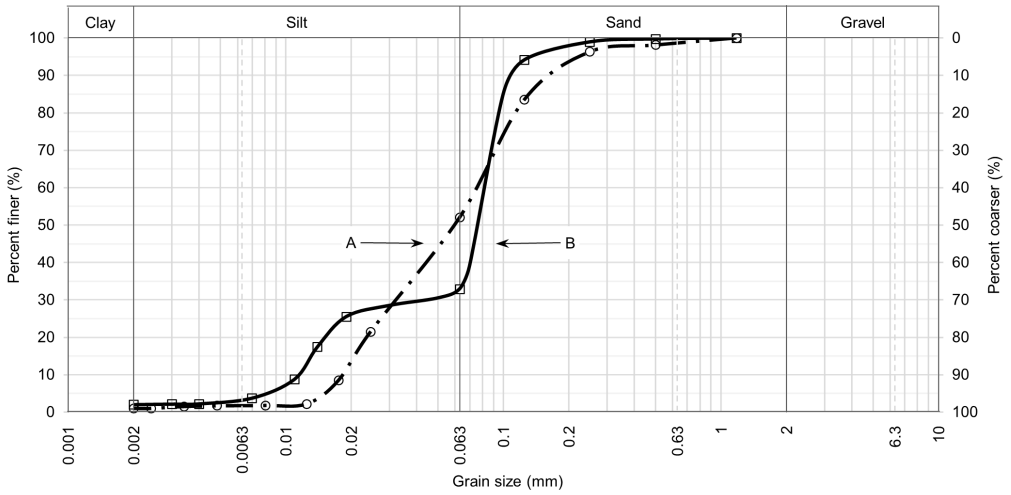

Figure 1. Grain size distribution of tested fly ash (A) and natural silty sand (B).

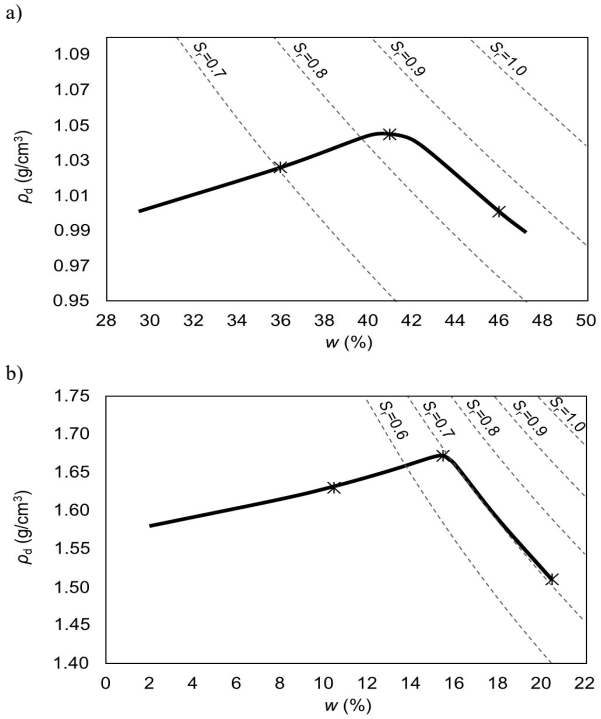

Figure 2. Compaction curves of samples with marked points corresponding to the water contents $w_{opt} \pm 5\%$: a) fly ash, b) silty sand.

Table 1. Parameters of the tested samples.

Material	Sample	w (%)	ρ_d (g/cm³)	n (%)	e (−)	S_r (−)
Fly ash	w_{opt} − 5%	36.0	1.026	51.6	1.066	0.715
	w_{opt}	41.0	1.045	50.7	1.029	0.844
	w_{opt} + 5%	46.0	1.001	52.8	1.118	0.972
Silty sand	w_{opt} − 5%	10.5	1.632	39.2	0.644	0.437
	w_{opt}	15.5	1.672	37.6	0.603	0.689
	w_{opt} + 5%	20.5	1.510	43.6	0.774	0.710

Structure was observed during microstructural studies of the natural fracture surface of the sample, without its drying or coating. The view field of the analyzed samples was approximately 550 μm in diameter for fly ash and 840 μm for silty sand, serving as a representative for the structure of the tested samples (Figure 3). The microstructure images were taken at magnifications of 2000x for fly ash and 750x or 1000x for silty sand to compare the microstructure at different water contents, $w_{opt} \pm 5\%$.

3 TEST RESULTS

Samples of fly ash and silty sand differ not only in grain shape and density at various water contents during compaction but also mainly in pore distribution at a given water content. This difference is clearly visible in the view fields in Figure 3. A more detailed analysis of ESEM images, including pore measurements, allows for a qualitative assessment of pore distribution. It should be noted that direct analysis of ESEM images does not account for very small pores.

A detailed analysis of images at 2000x magnification was presented in (Zabielska-Adamska et al. 2019). Fly ash compacted on the dry side of the optimum water content consists of aggregates separated by pore spaces ranging from 1.35 to 82.28 μm. When compacted at the optimum water content, fly ash forms a denser structure with pore sizes between 5.79 and 27.28 μm and the fewest pores. The structure of fly ash compacted on the wet side of the optimum is noticeably looser, although its pore size does not differ greatly from the sample compacted at w_{opt}, with pore sizes from 1.21 to 27.28 μm. Silty sand images at 750x or 1000x magnification show that silty sand compacted at w_{opt} − 5% has a rather loose structure with pore sizes from 8.157 to 111.90 μm. Similar values are seen for the sample compacted at w_{opt} + 5%, where pore sizes range from 5.154 to 112.800 μm; however, this sample appears more compact and requires higher magnification for detailed evaluation. Visibility of pores is less frequent. For fly ash compacted at the dry and wet sides of the optimum, the differences in structure are not significant. The median pore sizes are 24.44 μm and 12.69 μm for fly ash, and 31.53 μm and 21.59 μm for silty sand, respectively, for samples compacted at the dry and wet sides. The most noticeable difference is observed in the sample compacted at the optimum water content, with pore sizes ranging from 9.283 to 230.60 μm. Interestingly, the sample characterized by the highest dry density (Table 1) shows the largest pore sizes, likely due to discontinuities in the silty sand's grain size. Median pore sizes are 12.71 μm for fly ash and 42.865 μm for silty sand.

Figures 4–6 show ESEM images of silty sand samples compacted at three different water contents. The largest number of images is presented for the optimally compacted silty sand (Figure 5), because the greatest differences in the microstructure of fly ash and silty sand are observed in samples compacted at the optimum water content. In Figure 5, the large pore spaces are evident.

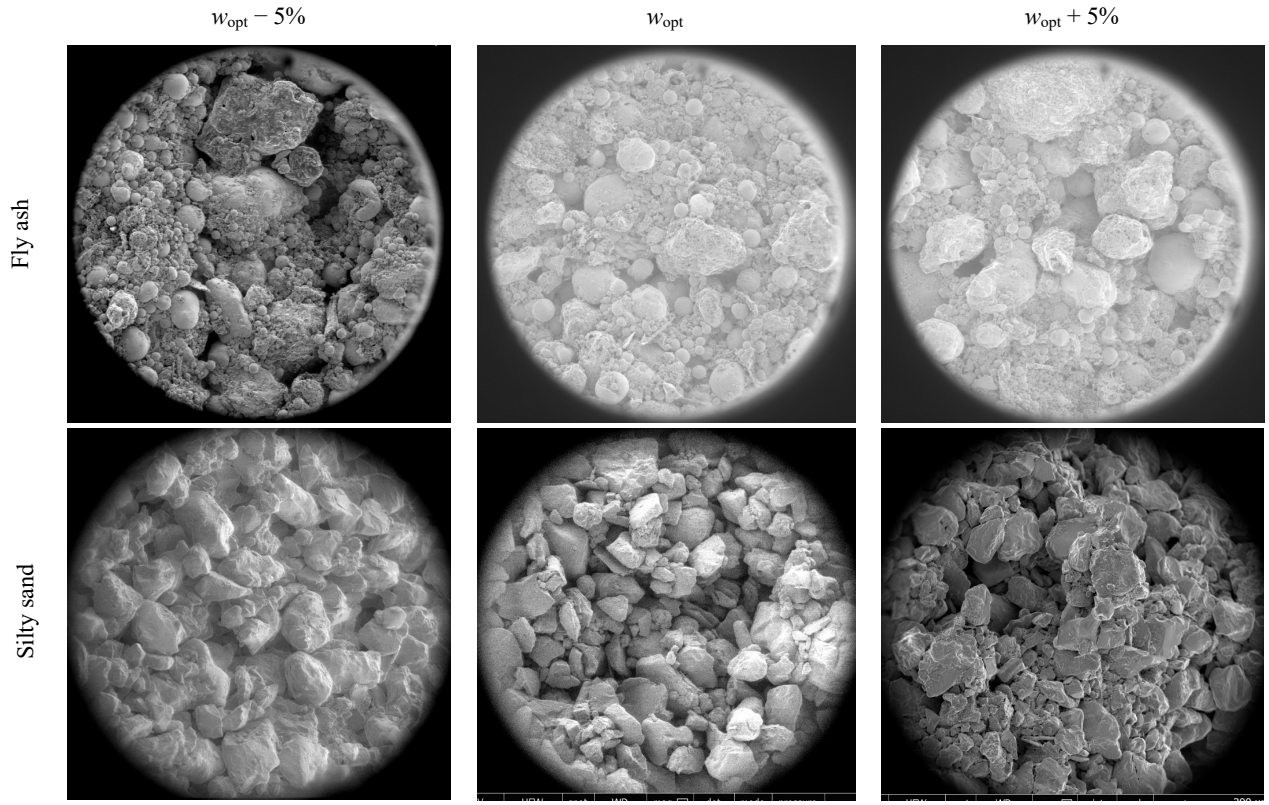

Figure 3. ESEM images of compacted fly ash (magn. 350x) and silty sand (magn. 300x) at compaction water content $w_{opt} \pm 5\%$.

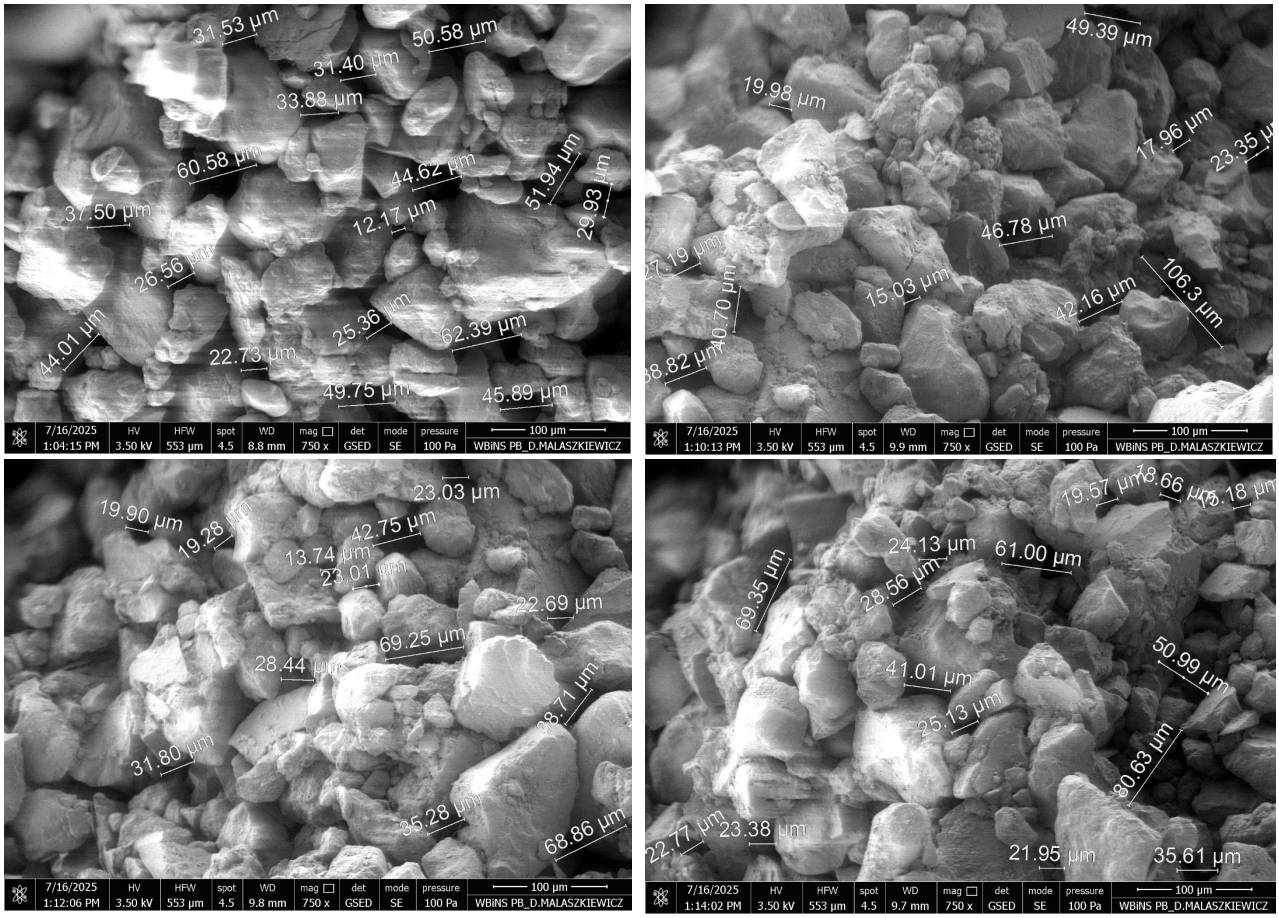

Figure 4. ESEM images (magn. 750x) of silty sand compacted at w_{opt} − 5%.

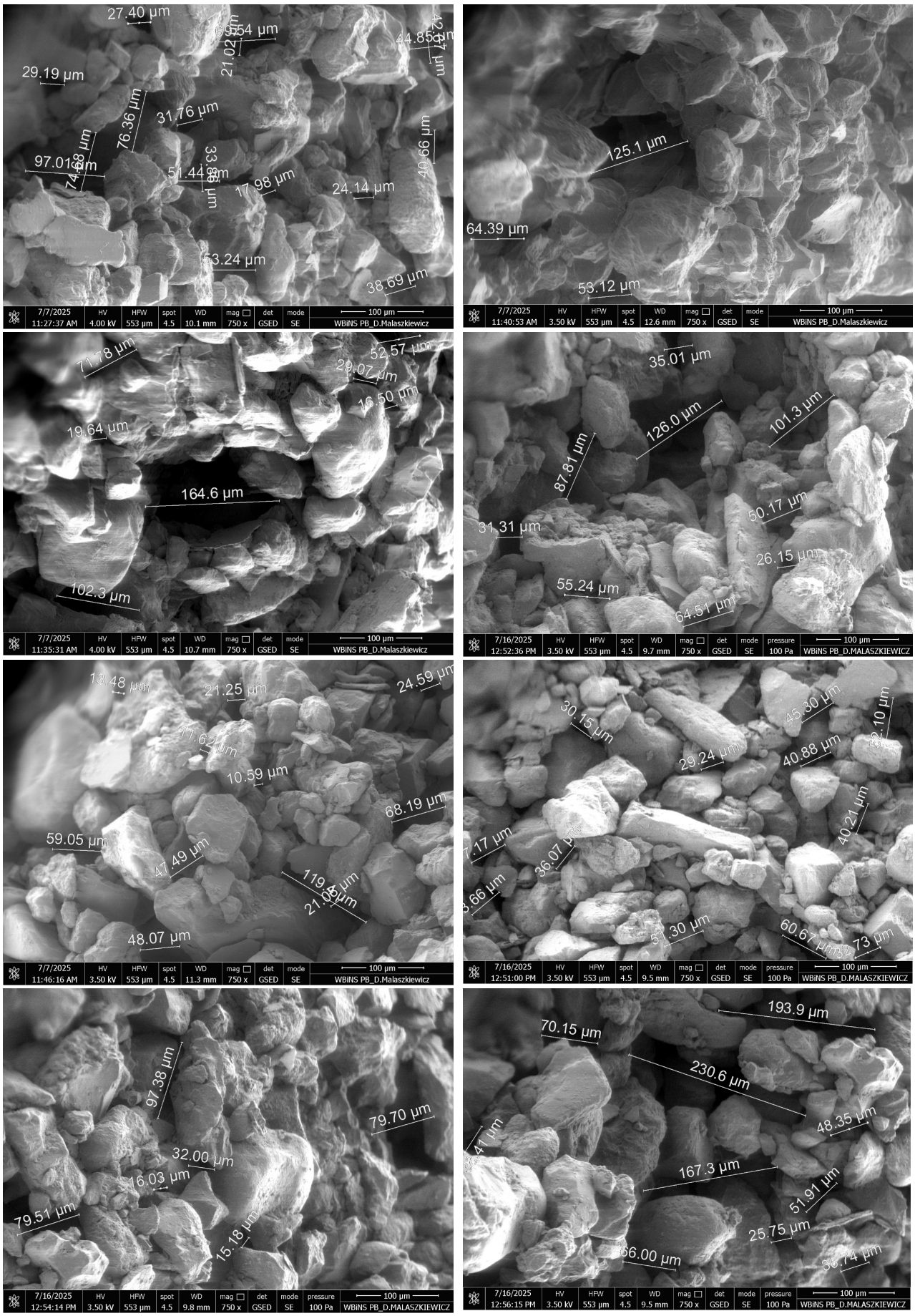

Figure 5. ESEM images (magn. 750x) of silty sand compacted at w_{opt}.

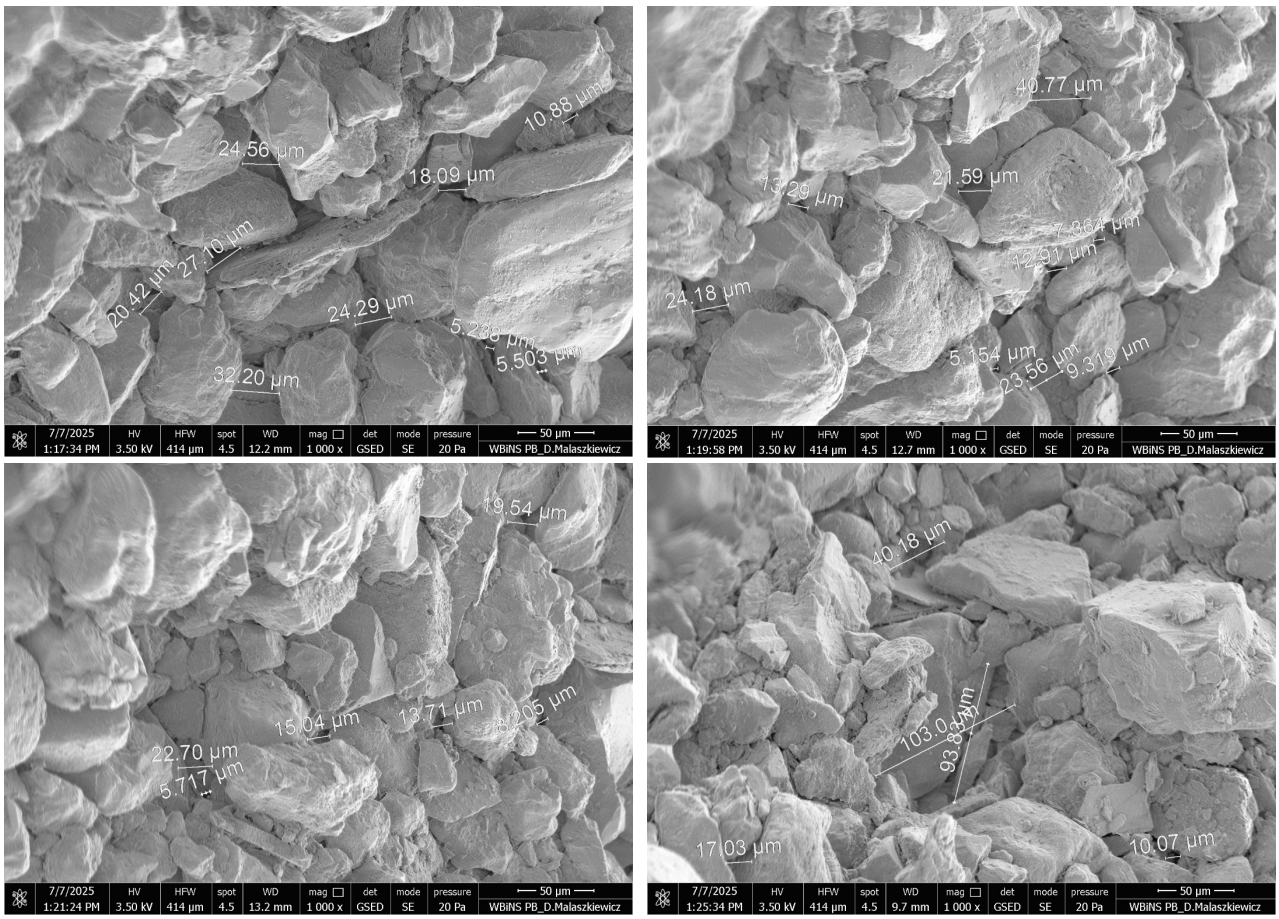

Figure 6. ESEM images (magn. 1000x) of silty sand compacted at w_{opt} + 5%.

Figure 7 presents the statistical analysis of the measured pore space for all fly ash and silty sand samples, including range results and median values, while Figure 8 shows pore distribution histograms for silty sand samples.

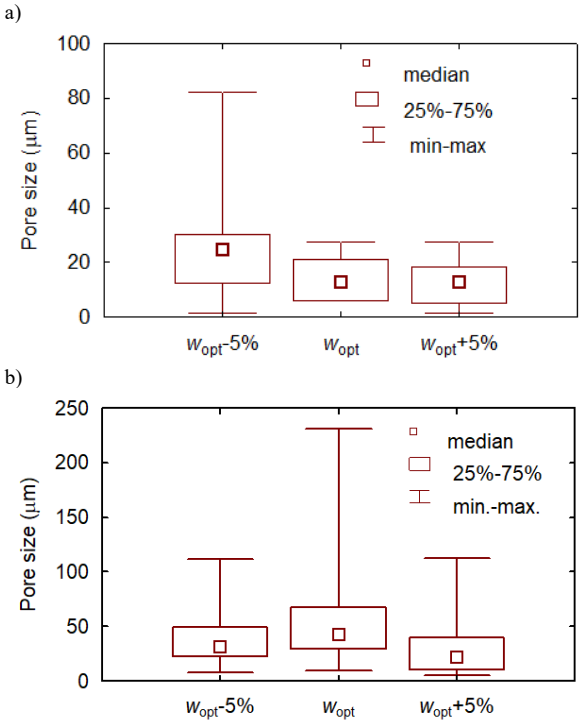

Figure 7. The statistical analysis of measurable pore space for all samples: a) fly ash, b) silty sand.

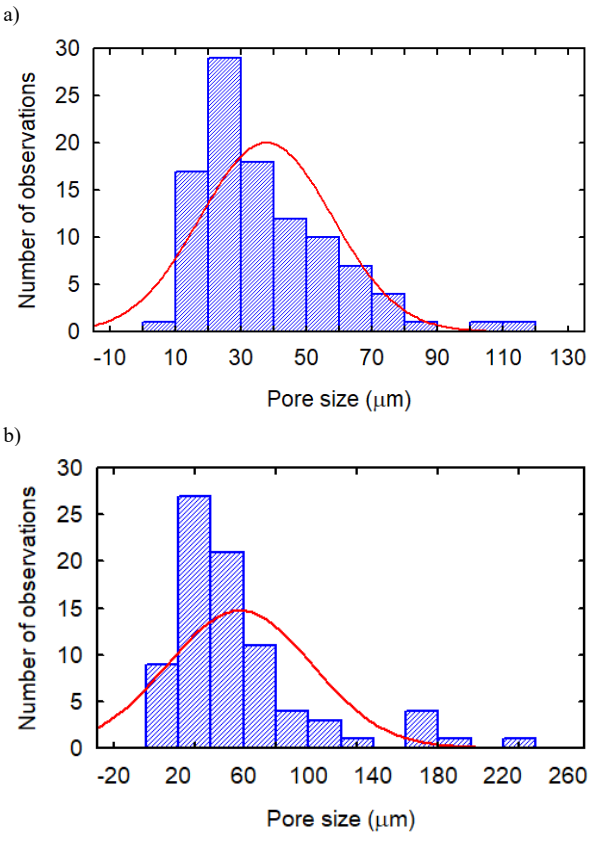

c)

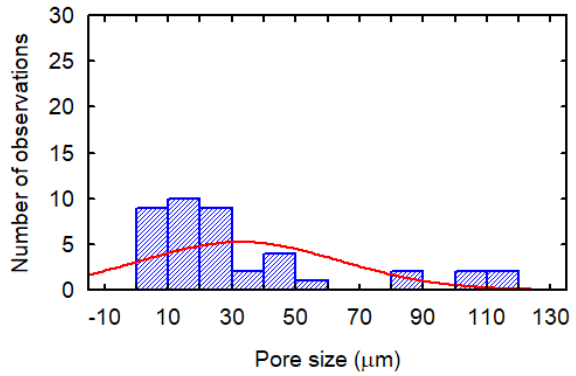

Figure 8. Pore size distribution for silty sand: a) w_{opt} – 5%, b) w_{opt}, c) w_{opt} + 5%.

The analysis of pore size distribution histograms (Figure 8) does not give a clear answer about the "transitional" nature of silty sand, which is visible in the case of fly ash. However, the discontinuity in grain size distribution of natural silty sand is evident (gap grading), which is manifested in large pore spaces formed during compaction at the optimum water content.

4 CONCLUSIONS

The paper demonstrates the potential of applying the ESEM technique to assess the microstructure of compacted wet transitional soils.

The most important achievement of this work is the demonstration of how grain size discontinuity affects the structure of compacted silty sand. Analysis of ESEM images revealed large pore spaces in the structure of gap-graded silty sand compacted at optimum water content.

The ESEM images confirmed the transitional nature of the fly ash. The structure of the tested fly ash closely resembles that of cohesive soils, exhibiting a multi-modal pore size distribution in samples compacted at $w \leq w_{opt}$ and a unimodal distribution in samples compacted at $w > w_{opt}$.

The transitional behavior of silty sand is not clearly stated, as a structure with well-defined large macro-pores and small pores within the aggregates has not been observed, similar to cohesive soil.

5 ACKNOWLEDGEMENTS

This work, carried out in 2025 at the Bialystok University of Technology, was supported by Polish financial resources for science.

6 REFERENCES

Cubrinovski, M., and Ishihara, K. 2002. Maximum and minimum void ratio characteristics of sand. Soils and Foundations 42(6), 65–78.

Delage, P., Audiguier, M., Cui, Y.J., and Howat, M. 1996. Microstructure of a compacted silt. *Canadian Geotechnical Journal* 33, 150–158.

Kwa, K.A., and Airey, D.W. 2016. Critical state interpretation of effects of fines in silty sands. *Géotechnique Letters* 6, 100–105.

Lade, P.V., Liggio, C.D., and Yamamuro, J.A. 1998. Effect of non-plastic fines on minimum and maximum void ratios of sand. *Geotechnical Testing Journal* 21(4), 336–347.

Nocilla, A., Coop, M.R., and Colleselli, F. 2006. The mechanics of an Italian silt: an example of 'transitional' behavior. *Géotechnique* 56(4), 261–271.

Polito, C.P., and Martin II, J.R. 2001. Effects of nonplastic fines on the liquefaction resistance of sands. *Journal of Geotechnical and Geoenvironmental Engineering* 127(5), 408–415.

Ponzoni, E., Nocilla, A., and Coop, M.R. 2017. The behaviour of gap graded sand with mixed mineralogy. *Soils and Foundations* 57(6), 1030–1044.

Romero, E. 2013. A microstructural insight into compacted clayey soils and their hydraulic properties. *Engineering Geology* 165, 3–19.

Tarantino, A., and De Col, E. 2008. Compaction behavior of clay. Géotechnique 58, 199–213.

Zabielska-Adamska, K. 2020. Characteristics of compacted fly ash as a transitional soil. *Materials* 13(6), 1387.

Zabielska-Adamska, K., Małaszkiewicz, D., and Konopko, M. 2019. Microstructure of compacted fly ash. *Proc. 17th European Conference on Soil Mechanics and Geotechnical Engineering*, Reykjavik.

ASTM International, 2024. ASTM D653-24 *Standard terminology relating to soil, rock, and contained fluid*. West Conshohocken: ASTM.

ASTM International, 2025. ASTM D2487-17 *Standard practice for classification of soils for engineering purposes (Unified soil classification system)*. West Conshohocken: ASTM.

European Committee for Standardization, 2018. EN ISO 14688-1 *Geotechnical investigation and testing – Identification and classification of soil – Part 1: Identification and description*. Brussels: CEN.

European Committee for Standardization, 2018. *EN ISO 14688-2 Geotechnical investigation and testing – Identification and classification of soil – Part 2: Principles for a classification.* Brussels: CEN.